A Comparison of Extreme Structural Responses and Fatigue Damage of Semi-submersible Type Floating Horizontal and Vertical Axis Wind Turbines

Zhengshun Cheng[a,b,c,*], Helge Aagaard Madsen[d], Wei Chai[a], Zhen Gao[a,b,c], Torgeir Moan[a,b,c]

[a] *Department of Marine Technology, Norwegian University of Science and Technology (NTNU), Trondheim, NO-7491, Norway*
[b] *Centre for Ships and Ocean Structures (CeSOS), NTNU, Trondheim, NO-7491, Norway*
[c] *Centre for Autonomous Marine Operations and Systems (AMOS), NTNU, Trondheim, NO-7491, Norway*
[d] *Department of Wind Energy, Technical University of Denmark, Roskilde, 4000, Denmark*

Abstract

Currently development of floating wind turbines for deep water is mainly based on horizontal axis wind turbines (HAWTs). However, vertical axis wind turbines (VAWTs) are possible alternative due to their potential in the cost of energy reduction. This study deals with a comparison of stochastic dynamic responses of floating HAWTs and VAWTs with emphasis on the extreme structural responses and fatigue damages. A 5 MW three-bladed HAWT and three 5 MW VAWTs with blade number ranging from two to four were mounted on a semi-submersible platform. Their stochastic dynamic responses, short-term extreme structural responses and fatigue damages were estimated in both operational and parked conditions. The results show that the three- and four-bladed floating VAWTs and the three-bladed floating HAWTs considered have similar performances in the variation of generator power production, in the maximum tower base bending moment and in the fatigue damages at tower base and mooring lines. However, the maximum tensions in mooring line for the three- and four-bladed floating VAWTs are approximately four times higher than that of floating HAWTs, which implies a significant challenge for their mooring sys-

*Corresponding author. Email address: zhengshun.cheng@ntnu.no

tems. The maximum tower base bending moment and fatigue damage in the two-bladed floating VAWT are extremely significant.

Keywords: floating wind turbine, horizontal axis wind turbine, vertical axis wind turbine, extreme structural response, fatigue damage

1. Introduction

Currently, harvesting the offshore wind resources in intermediate and deep water using floating horizontal axis wind turbine (HAWT) concepts is facing the challenge of much higher cost of energy than the present onland or near-shore technology. New alternative technology that can reduce the cost of energy in deep water is required for future wind energy market. Due to its lower center of gravity, independence of wind direction, reduced machine complexity and excellent potential to reduce the cost of energy compared with the floating HAWT [1], the floating vertical axis wind turbine (VAWT) is a very promising alternative to harvest offshore wind energy resources.

A large amount of effort was devoted to develop VAWTs, mainly in the USA and Canada, during the 1970s and 1980s [2]. And the VAWT was once commercialized in the USA in the 1980s. More than 500 turbines were installed in California's Altamont and Tehachapi passes, and the total installed capacity reached 95 MW by the end of 1985. Unfortunately, the FloWind Corporation went bankrupt in 1997 due to fatigue failures within the blades. After that, the VAWTs gradually lost the competition with the HAWTs in the commercial market. The fatigue issue of the VAWT is usually caused by periodically varying aerodynamic loads, especially for VAWTs with two blades. Currently, it can be overcome by the use of modern composite materials [3]; it can also be alleviated by increasing the blade number [4], using helical blades, or employing a more advanced control strategy. In addition, employing a catenary moored floating substructure can help to mitigate the fatigue damage at tower base suffered by the onshore VAWTs as well [5].

Therefore, it seems that the VAWT can to some extent compete with the HAWT in intermediate and deep water where a floating wind turbine is more economical. The interest in the development of VAWTs for offshore application has thus been resurging. The state-of-the-art floating VAWT concepts, fully coupled aero-hydro-servo-elastic simulation tools for floating VAWTs, and dynamic response characteristics of floating VAWTs in operational, parked and fault conditions are reviewed by Cheng in his PhD thesis [6].

To reveal the merits and feasibilities of floating HAWTs and floating VAWTs, a number of comparative studies have been conducted. Paraschivoiu [2], Eriksson et al. [7] and Borg et al. [8] described and compared the onshore HAWTs and VAWTs; however, integrated dynamic analyses are not considered. Borg and Collu [9] carried out a preliminary comparison between the floating HAWT and VAWT based on prime principles with emphasis on the aerodynamic forces and their impact on the static and dynamic responses. But limited comparison regarding the dynamic behavior was conducted and no structural elasticity and controller were included for the floating VAWT.

Wang et al. [10] and Cheng et al. [11, 12] conducted more comprehensive comparisons on the performance and dynamic responses of floating HAWTs and VAWTs using the fully coupled aero-hydro-servo-elastic simulations. Wang et al. [10] performed a comparative study on the dynamic responses of a floating VAWT with the DeepWind 5 MW two-bladed Darrieus rotor [13] and a floating HAWT with the NREL 5 MW three-bladed HAWT [14], both mounted on a semi-submersible platform. Cheng et al. [11] studied the same rotors with a spar buoy subjected to constant wind. However, the wind fields were created with respect to different reference heights for the floating HAWT and VAWT, which implies that a slightly different wind field was used, though its effect was very small. Moreover, the generator power of the floating VAWT exceeds 5 MW above the rated wind speed and could even reach up to 9 MW. Thus, an improved control strategy [12] was proposed to hold the generator power approximately constant as that of the HAWT above the rated wind speed. This control strategy was achieved by adjusting the generator torque. A

more comprehensive comparative study was conducted by Cheng et al. [12] and indicated that due to different aerodynamic load characteristics and control strategies, the current design of the spar-type VAWT leads to larger mean values and standard deviations in the tower and mooring lines and requires further improvements.

Nonetheless, the studies conducted by Wang et al. [10] and Cheng et al. [11, 12] employed a two-bladed Darrieus rotor for the floating VAWTs and identified the prominent 2P (twice-per-revolution) frequency component in the structural responses of the floating VAWTs, which is caused by the periodic varying aerodynamic loads due to the two blades. Cheng et al. [4] has demonstrated that the structural responses are strongly dependent on the number of blades and increasing the number of blades from two to three can significantly reduce the variation in structural responses, for instance the tower base bending moment. Therefore, it is of great interest to conduct a comparative study of floating HAWTs and VAWTs with identical blade number.

In practice, the ultimate limit state (ULS) and fatigue limit state (FLS) are usually considered in the design of a floating wind turbine system. Hence, the extreme structural responses and fatigue damage, which are relevant for the ULS and FLS design respectively, are ideal parameters for the assessment of performance of floating HAWTs and VAWTs. In this study, the stochastic dynamic responses of floating HAWTs and floating VAWTs are studied and compared under normal operational and parked conditions. The floating HAWTs with the NREL 5 MW three-bladed HAWT [14], and the floating VAWTs with straight and parallel blades and with blade number ranging from two to four [4], both mounted on the OC4 semi-submersible platform [15], were considered. Their stochastic responses were estimated by carrying out fully coupled time domain simulations under correlated turbulent wind and irregular waves. These floating HAWTs and VAWTs have similar generator power production performance above the rated wind speed. Their structural responses are compared in terms of extreme structural responses and damage equivalent fatigue loads (DEFLs).

This paper is organized as follows. The floating wind turbine models are

first introduced in section 2. The methodology used is described in section 3, including the fully coupled analysis method, extreme value estimation method and fatigue damage estimation method. By defining a series of load cases in section 4, the comparative studies of the floating HAWTs and VAWTs were conducted with respect to the stochastic dynamic responses, extreme structural responses and DEFLs in section 5.

2. Floating Wind Turbine Models

In this study, one floating HAWT and three floating VAWTs, both mounted on a semi-submersible platform, were considered in water with a depth of 200 m, as illustrated in Figure 1.

The floating HAWT employs the NREL 5 MW wind turbine, which is a traditional three-bladed upwind HAWT [14]. The floating VAWTs use three H-type rotors with parallel and straight blades. These three H-rotors have identical solidity while the number of blades varies from two to four. And they are designed to achieve a rated power of 5 MW, which is the same as the HAWT [4], as shown in Figure 2. The main specifications of the HAWT and VAWTs are given in Table 1. The HAWT and VAWTs have identical cut-in and cut-out wind speeds, but a different rated wind speed and rated rotational speed. Moreover, the nacelle of the HAWT is placed at the tower top while that of the VAWT is assumed to be located at the tower base. The rotor mass and its center of mass present some difference for the HAWT and VAWTs as well.

Both the HAWT and VAWTs were mounted on the same semi-submersible platform with three catenary mooring lines. The semi-submersible platform was originally designed to support the NREL 5MW wind turbine in the OC4 project [15], which is the floating HAWT concept considered here. It was modified to support these three VAWTs by adjusting the ballast [4]. Due to the difference in rotor mass between the NREL 5MW wind turbine and the H-type VAWTs, the ballast of the semi-submersible platforms for the floating VAWTs was adjusted to maintain the same draft and displacement as that of the floating HAWT.

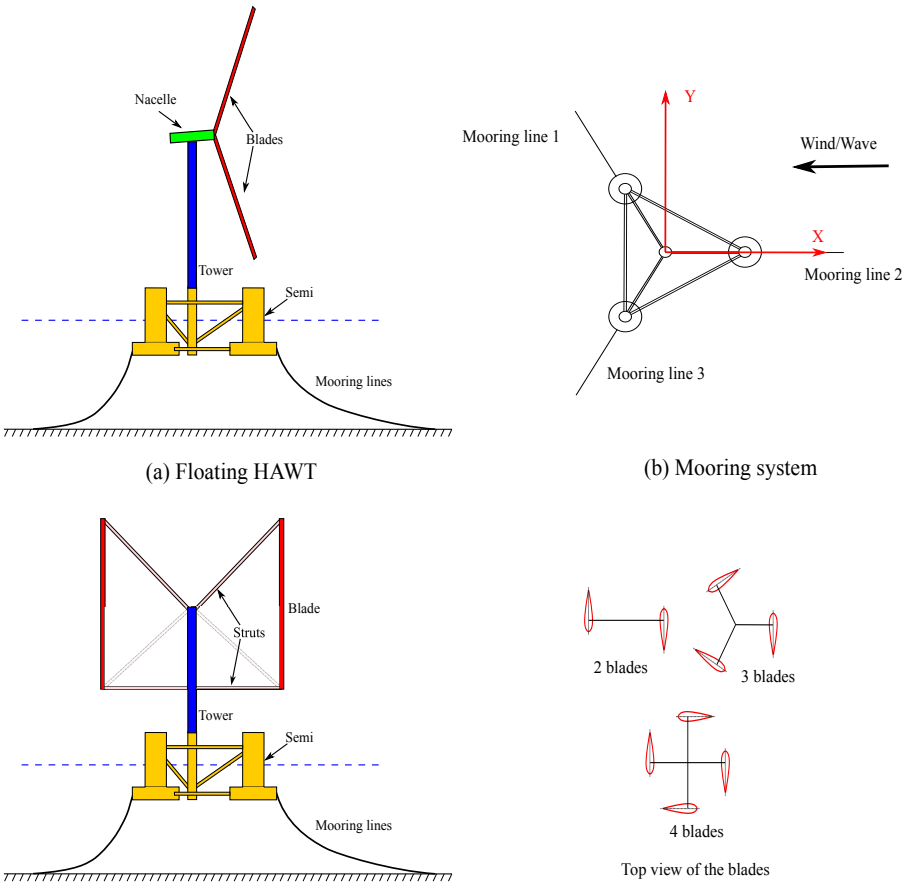

Figure 1: Illustration of floating wind turbine models. (a) floating horizontal axis wind turbine (HAWT), (b) mooring system, (c) floating vertical axis wind turbine (VAWT). The platform and the wind turbines are not in the same scale. For floating VAWTs, the top view of the blades that corresponds to an azimuth angle of 0° is also illustrated, and the azimuth angle are defined in clockwise direction.

Table 1: Specifications of HAWT and VAWTs

Turbines	HAWT	VAWT H2	VAWT H3	VAWT H4
Rated power [MW]	5	5.21	5.30	5.35
Number of blades [-]	3	2	3	4
Rotor radius [m]	63	39.0	39.0	39.0
Tower top height [m]	90	79.78	79.78	79.78
Chord length [m]	1.419-4.652	4.05	2.7	2.03
Cut-in, rated, cut-out wind speed [m/s]	5 , 11.4 , 25	5 , 14 , 25	5 , 14 , 25	5 , 14 , 25
Rated rotor rotational speed [rpm]	12.1	10.3	10.3	10.3
Nacelle mass [ton]	240	0	0	0
Rotor mass, including blades, struts, tower and shaft [ton]	359.7	350.1	315.3	287.7
Center of mass for rotor [m]	(-0.2 , 0 , 70.06)	(0, 0, 51.03)	(0, 0, 48.14)	(0, 0, 45.34)

Table 2: Properties of the floating wind turbine systems

	HAWT	VAWT H2	VAWT H3	VAWT H4
Water depth [m]	200	200	200	200
Draft [m]	20	20	20	20
Diameter at mean water line [m]	12.0/6.5	12.0/6.5	12.0/6.5	12.0/6.5
Platform mass, including ballast [ton]	13473	13761.3	13796.1	13823.7
Center of mass for platform [m]	(0, 0, -13.51)	(0, 0, -13.44)	(0, 0, -13.43)	(0, 0, -13.43)
Buoyancy at the equilibrium position [kN]	139816	139816	139816	139816
Center of buoyancy [m]	(0, 0, -13.15)	(0, 0, -13.15)	(0, 0, -13.15)	(0, 0, -13.15)
Surge/Sway [s]	112.0	113.15	113.15	113.15
Heave [s]	17.1	17.04	17.04	17.04
Pitch/Roll [s]	25.8	21.17	20.68	20.32
Yaw [s]	80.2	80.38	80.44	80.49

Since the difference in rotor mass between the HAWT and VAWTs is very small compared with the displacement of the platform, it is thus assumed that such modification will not affect the hydrostatic performance. Main properties of the floating HAWT and VAWTs are given in Table 2. It should be noted that the platform mass of floating VAWTs includes steel weight, ballast as well as the generator weight. The natural periods of rigid-body motions of floating HAWT and VAWTs are numerically estimated by conducting free decay tests. More detailed information about the semi-submersible platform and how to adjust the ballast are described by Robertson et al. [15] and Cheng et al. [4], respectively.

3. Methodology

3.1. Fully coupled analysis methods

Two fully coupled codes, the SIMO-RIFLEX-AeroDyn [16] and SIMO-RIFLEX-AC [17], were used to carry out the integrated dynamic analysis of floating HAWTs and VAWTs in time domain, respectively. Both codes can account for the turbulent wind field, aerodynamics, hydrodynamics, structural dynamics, mooring line dynamics and control system dynamics. These two codes are based on the SIMO [18] program and RIFLEX [19] program that were developed by MARINTEK and have been widely used in the offshore oil and gas industry. For each fully coupled code, three computer programs are integrated. SIMO [18] computes the hydrodynamic loads acting on the platform hull based on a combination of the potential flow theory and Morison's equation; RIFLEX [19] represents the blades, tower, shaft, struts and mooring lines as flexible finite elements and provides links to an external controller and an aerodynamic code. The aerodynamic code, AeroDyn or AC, calculates the aerodynamic loads acting on the blades. External control systems were also implemented for each coupled code. The main difference between these two coupled codes lies in the control strategy and the method for computing the aerodynamic loads.

The floating HAWT was modeled by using the SIMO-RIFLEX-AeroDyn code, which was developed by Ormberg and Bachynski [16]. The program AeroDyn, developed by NREL [20], is employed to calculate the forces and moments on the blades according to the Blade Element Momentum (BEM) theory or the Generalized Dynamic Wake (GDW) theory. The aerodynamic drag forces on the tower is modeled based on the potential flow theory. The external control system is used to regulate both the rotational speed and blade pitch angle. It employs the generator torque controller below the rated wind speed and the blade pitch controller above the rated wind speed. The SIMO-RIFLEX-AeroDyn code has been verified by comparing it with FAST and other comprehensive codes [16, 21].

The floating VAWTs were modeled by using the SIMO-RIFLEX-AC code,

which was developed by Cheng et al. [17]. The program AC calculates the aerodynamic loads acting on the blades based on the Actuator Cylinder (AC) flow method, which is originally developed by Madsen [22] and further discussed and detailed by Cheng et al. [23]. The effects of dynamic inflow as well as dynamic stall using the Beddoes-Leishman model are included in the AC code. However, the drag forces acting on the tower and struts are neglected [4]. Moreover, by assuming a fixed blade pitch angle for large VAWTs, a generator torque controller based on a proportional-integral-derivative (PID) algorithm is implemented to regulate the rotor rotational speed. The program AC has been validated with experiment results [23] and the SIMO-RIFLEX-AC code has been verified by a series of numerical comparisons with other computer codes [17].

For the floating HAWT and floating VAWTs considered in this study, the hydrodynamic loads were computed in SIMO by applying the potential flow theory and Morison's equation. The potential flow theory was applied for the platform hull. The added mass, radiation damping and first order wave excitation forces were firstly estimated in the frequency domain and then applied in the time domain by using the convolution technique [24]. Additional viscous force on the hull was included by the Morison's formula. Morison's formula was also applied for slender structures, such as the braces and mooring lines.

In the structural model, the semi-submersible platform including the braces were represented as a rigid body; the blades, tower, shaft and mooring lines were modeled using flexible nonlinear finite elements. A flexible joint was introduced to connect the rotating shaft and non-rotating parts. The generator torque can be applied through this point to regulate the rotor rotational speed. In this way, the dynamic equilibrium equations of the floating wind turbine systems were solved in the time domain using the Newmark-β integration method ($\beta = 0.256$, $\gamma = 0.505$). Structural damping was included through global proportional Rayleigh damping terms for all beam elements.

3.2. Extreme value estimation

In practice, the extreme value of structural responses at certain components is of great concern since it is relevant for ULS design. In this study, it is considered based on the mean up-crossing rate method [25]. The mean up-crossing rate is a key parameter for the extreme response statistics as well as for evaluation of the associated reliability of marine structures.

The extreme value is the maximum in a set of a finite number of independent and identically distributed random variables. For high response levels, if the assumption of statistically independent upcrossing is valid, it is reasonable to assume that the random number of upcrossing in an arbitrary time interval of length T is approximately Poisson distributed. If the response process is not too narrow banded, this is a reasonable assumption. Let $M(T) = max\{Y(t); 0 \leq t \leq T\}$ denotes the extreme value for the random process $Y(t)$ over a duration $[0, T]$, then the extreme value distribution is given by

$$P\left(M(T) \leq y\right) = exp\left(-\int_0^T v^+(y;t)dt\right) \tag{1}$$

where $v^+(y;t)$ is the up-crossing rate of the level y. The up-crossing rate of a process at a defined level is the average frequency of the positive slope crossings of that level. For a stationary short-term process, rewriting Eq. 1 in terms of the mean up-crossing rate $\bar{v}^+(y) = \frac{1}{T}\int_0^T v^+(y;t)dt$, the probability of exceedance of a defined level y is

$$P\left(M(T) > y\right) = 1 - exp\left(-\bar{v}^+(y)T\right) \tag{2}$$

The mean up-crossing rate can be directly estimated from simulated time series. Let $n^+(y;T)$ denotes the counted number of upcrossings during the time interval $[0, T]$ for a particular time history, then the sample mean value estimation of $v^+(y)$ for k time histories of duration T is given by

$$\hat{\bar{v}}^+(y) = \frac{1}{kT}\sum_{j=1}^{k} n_j^+\left(y;T\right) \tag{3}$$

where $n_j^+(y;T)$ denotes the number of upcrossings of the level y by the jth time history during $[0,T]$. For a suitable number k, a good approximation of the 95% confidence interval (CI) would be

$$\mathbf{CI}_{\pm}(y) = \hat{\bar{v}}^+(y) \pm \frac{1.96\hat{s}(y)}{\sqrt{k}} \tag{4}$$

where $\hat{s}(y)$ is the empirical standard deviation and is given as

$$\hat{s}(y)^2 = \frac{1}{k-1}\sum_{j=1}^{k}\left(\frac{n_j^+(y;T)}{T} - \hat{\bar{v}}^+(y)\right)^2 \tag{5}$$

Eqs. (3)-(5) describes the empirical estimation of the mean upcrossing rate obtained by direct numerical simulations (i.e. Monte Carlo simulation). However, direct numerical calculations require extensive time resources to evaluate the statistics of extreme responses that correspond to low probability levels [26]. Nevertheless, an extrapolation technique is applied in order to circumvent this obstacle.

The extrapolation technique is based on the observation that for marine structures, the mean upcrossing rate as a function of level y is in general highly regular in a specific way in the tail region. For a wide range of dynamical systems, the mean upcrossing rate tail (e.g. $y \geq y_0$) behaves similarly to $\exp\{-a(y-b)^c\}$, where $a > 0$, $b \leq y_0$ and $c > 0$ are suitable constants. The mean up-crossing rate is therefore assumed to be in the form of

$$\bar{v}^+(y) = q(y)exp\left\{-a\left(y-b\right)^c\right\}, y \geq y_0 \tag{6}$$

where the function $q(y)$ is slowly varying compared with the exponential function $exp\left\{-a\left(y-b\right)^c\right\}$ for tail values of y. Under the aforementioned assumptions, plotting $\log|\log v^+(y)/q(y)|$ versus $\log(y-b)$ would give an almost perfectly linear tail behavior. In general, $q(y)$ is not constant, but its variation in the tail region is usually sufficiently slow to allow for its replacement by a constant [27]. The Levenberg-Marquardt least squares optimization method is used to determine the optimal values for a, b, c and q. Detais of this method can refer to Naess et al. [28] and Naess and Gaidai [27].

Extreme value statistics can be calculated with the assistance of the extrapolation technique based on the regularity of the mean upcrossing rate in the tail region. It has been shown that, with the advantage of the time-saving extrapolation technique, the proposed method does give a satisfactory estimation of the extreme responses with a significant reduction of the simulation time [29, 28].

3.3. Fatigue damage estimation

The stochastic wind and wave loads applied on the floating wind turbines can cause oscillations of structural responses at certain components, such as tower base and mooring line. In this study, the short-term fatigue damage of the wind turbine components is addressed. A Matlab-based computer program MLife, developed by NREL [30], is used to estimate the short-term damage equivalent fatigue loads (DEFLs) for each component.

The short-term DEFL is a constant-amplitude load that occurs at a fixed load-mean and frequency and can produce damage that is equivalent to that of the variable spectrum loads. The short-term DEFL is estimated based on the S-N curve method, and the rainflow counting algorithm is applied to count the cycle number corresponding to different mean loads and load ranges. The short-term DEFL is given by

$$\mathbf{DEFL}_j^{STF} = \left(\frac{\sum_i \left(n_{ji} (L_{ji}^{RF})^m \right)}{n_j^{STeq}} \right)^{\frac{1}{m}} \tag{7}$$

where $n_j^{STeq} = f^{eq} T_j$ is the total equivalent fatigue counts for time-series j, f^{eq} is the DEFL frequency and T_j is the elapsed time of time-series j. m is the Wöhler exponent, n_{ji} is the cycle count and L_{ji}^{RF} is the cycle's load range about a fixed load-mean value of time-series j.

In this study, The DEFL frequency f^{eq} was assumed to be 1Hz. The Wöhler exponent m was set to be 3 for the tower base and mooring lines. Because the floating wind turbines considered are generalized concepts, fatigue damage analysis is performed without applying the Goodman correction.

4. Load cases and environmental conditions

A series of load cases (LCs) with turbulent wind and irregular waves were defined for the floating wind turbine systems and used in the time domain simulations, as given in Tables 3. The wind and wave are correlated and directionally aligned. LCs 1-8 are under normal operational condition. LC 9 is the extreme environmental condition and the wind turbines are parked. The HAWT is parked by pitching the blades in feather position. The VAWTs are parked with an azimuth angle that provides the smallest thrust on the rotor. These angles are 90°, 0° and 0° for the two-, three- and four-bladed VAWTs, respectively. It should be noted that there are certain deviations between the prescribed azimuth angle and the actual azimuth angle in the simulations, and these deviations are small.

Table 3: Load Cases –combined wind and waves

	U_w (VAWT) [m/s]	U_w (HAWT) [m/s]	T_I	H_s [m]	T_p [s]	Simulation length [s]
LC1	5	5.09	0.224	2.10	9.74	3600
LC2	8	8.14	0.174	2.55	9.86	3600
LC3	10	10.17	0.157	2.88	9.98	3600
LC4	12	12.20	0.146	3.24	10.12	3600
LC5	14	14.24	0.138	3.62	10.29	3600
LC6	18	18.31	0.127	4.44	10.66	3600
LC7	22	22.37	0.121	5.32	11.06	3600
LC8	25	25.43	0.117	6.02	11.38	3600
LC9	50	51.22	0.105	12.9	14.1	3600

The three dimensional turbulent wind fields were generated using the NREL's TurbSim program [31] according to the Kaimal turbulence model for IEC Class C [32]. It uses both normal wind profile and normal turbulence model. In the normal wind profile, the wind profile $U(z)$ at a height of z is given by the following power law

$$U(z) = U_{ref}\left(\frac{z}{z_{ref}}\right)^{\alpha} \tag{8}$$

where U_{ref} is the reference wind speed, z_{ref} the height of reference wind speed and α the power law exponent. The value of α was chosen to be 0.14 for the floating wind turbines according to IEC 61400-3 [32]. The values of z_{ref} were set to 90 m (hub height) and 79.78 m (vertical center of the blades) above mean sea level (MSL) for the floating HAWT and floating VAWTs, respectively. The significant wave height (Hs) and peak period (Tp) were set based on their correlations with the wind speed for the Statfjord site in the northern North Sea [33].

To obtain a more reasonable comparison between the floating HAWT and floating VAWT, the same wind field and wave history were applied to both the floating HAWT and floating VAWT. The reference wind speeds at hub height for the floating HAWT were computed based on those of the floating VAWT according to Eq. 8, as the U_w given in Table 3. For each LC, each simulation lasted 4600 s, in which the first 1000 s was removed to eliminate the start-up transient effects and to form a one-hour dynamic analysis. Five identical and independent one-hour simulations with different seeds for turbulent winds and irregular waves were carried out for each LC to reduce the stochastic variations.

5. Results and discussions

As aforementioned, the floating HAWT and floating VAWTs have identical cut-in and cut-out wind speeds, but a different rated wind speed. The rated wind speed for the floating HAWT and VAWT are 11.4 and 14 m/s, respectively. With respect to the floating HAWT, the generator torque controller is applied to regulate the rotor rotational speed for wind speeds below the rated one. The required generator torque is obtained based on a look-up table between the generator torque and rotational speed. Above the rated wind speed, a blade pitch controller based on a PID control algorithm is used to adjust the blade pitch angle in order to hold the generator power or generator torque approximately constant. In this study, the control strategies with constant power and with constant torque are considered for wind speeds above the rated

one. Due to these control strategies, the thrust of floating HAWT reaches the maximum at the rated wind speed, as shown in Figure 2b.

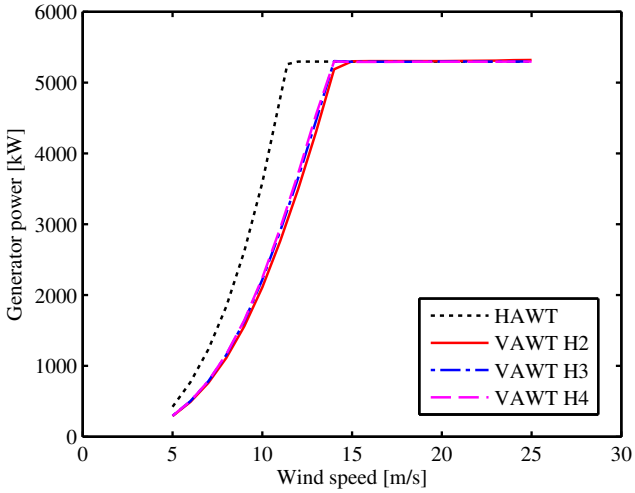

(a) Generator power

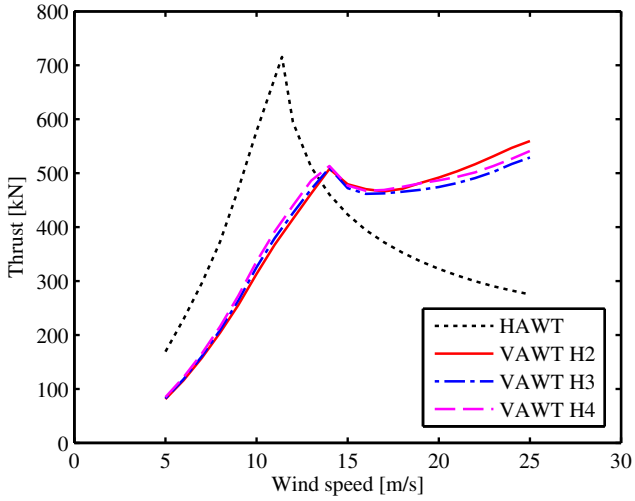

(b) Thrust

Figure 2: The steady-state generator power and thrust of the considered horizontal axis wind turbine (HAWT) and vertical axis wind turbines (VAWTs).

Regarding the floating VAWTs, a generator torque controller is used to regulate the rotor rotational speed for wind speeds ranging from the cut-in to the

cut-out. The required generator torque is updated based on a PID control algorithm which aims to minimize the error between the measured rotational speed and reference rotational speed. The reference rotational speed is chosen to maximize the power capturing below the rated wind speed and to maintain the generator power approximately constant above the rated wind speed. The curves of generator power and thrust are plotted in Figure 2.

It can be observed in Figure 2 that for wind speeds below 14 m/s the floating HAWTs can give a higher generator power and a larger thrust than the floating VAWTs. Regarding wind speeds above 14 m/s, the generator power between the floating HAWTs and VAWTs are very close, while the thrust of floating VAWTs is larger than that of floating HAWTs.

In this study, the stochastic dynamic responses of the above floating HAWTs and VAWTs are firstly studied and compared to demonstrate their dynamic response characteristics. The comparative study of floating HAWTs and VAWTs are further extended by analyzing the extreme structural responses and fatigue damages, which are relevant for the ULS design and FLS design, respectively.

5.1. Power production performance of floating HAWTs and VAWTs

The power production performance of the floating HAWTs and VAWTs is first studied. Figure 3 shows the mean values and standard deviations of the generator power of the floating HAWTs and VAWTs. The mean values of the generator power shown in Figure 3 follow the same trend as those steady state results shown in Figure 2, which implies that the implemented control strategies work well in both steady and turbulent wind conditions. For LCs 5-8, the mean values of the generator power of floating HAWTs and floating VAWTs are very close, while their standard deviations present notable differences. The standard deviations of the generator power of floating VAWTs, especially with two blades, are larger than those of floating HAWTs. The floating HAWT with constant power control strategy gives smallest standard deviation, especially for LCs 6-8. Moreover, in LCs 6-8, the standard deviation of the generator power of floating HAWTs with constant torque control strategy is comparable with

those of floating VAWTs with three and four blades.

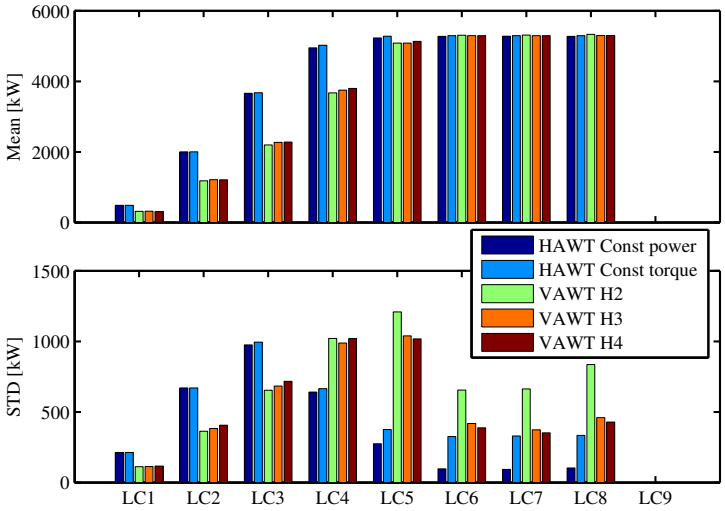

Figure 3: The mean value and standard deviation of generator power production for floating HAWT and VAWTs.

Given the distribution of mean wind speed, the annual power production of the floating HAWTs and VAWTs can be roughly estimated. The availability of these turbines is assumed to be 1. At the considered site [33], the marginal distribution of the mean wind speed at 10 m above the MSL can be described by a 2-parameter Weibull distribution :

$$F(U_W) = 1 - exp\left(-\left(\frac{u_w}{\beta}\right)^{\alpha}\right) \tag{9}$$

where α and β are the shape and scale parameters, respectively, and they were determined to be $\alpha = 1.708$ and $\beta = 8.426$ based on the measurements from the Northern North Sea in the period 1973-99. By using Eq. 8, the corresponding probability density function of the mean wind speed at the reference height of 79.78 m is computed and plotted in Figure 4. According to the mean generator power shown in Figure 3, the annual power production is approximately computed, as presented in Figure 5. The annual power production of floating VAWTs is about 16.8% less than that of floating HAWTs, because about 76% of the long-term wind speed is below 14 m/s and in this region the mean power

production of HAWTs is higher than that of VAWTs.

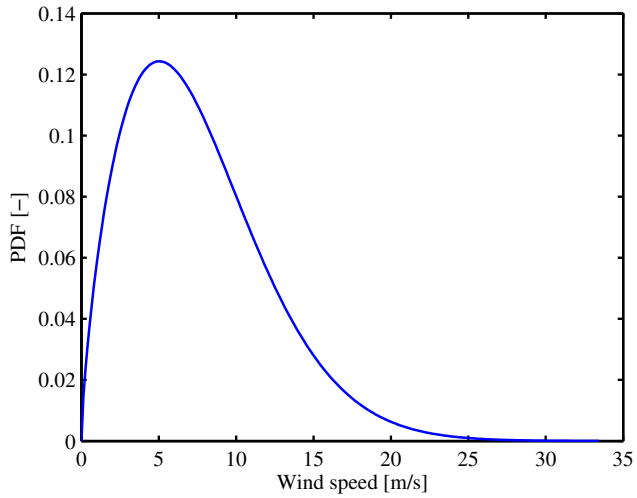

Figure 4: The probability density function (PDF) of the mean wind speed at the reference height of 79.78m.

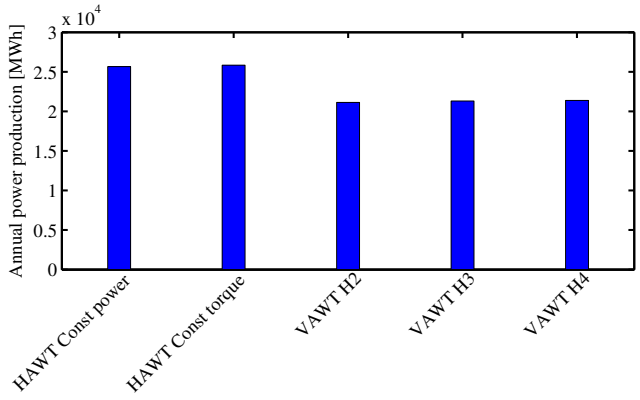

Figure 5: The estimated annual power production for the floating HAWTs and VAWTs.

5.2. Stochastic dynamic responses of floating HAWTs and VAWTs

The stochastic dynamic responses, such as the thrust and lateral force acting on the rotor, platform motions, tower base bending moments and mooring line tensions, of floating HAWTs and VAWTs were estimated under turbulent wind

and irregular waves. Both operational condition LCs 1-8 and parked condition LC9 were investigated.

Figure 6 shows the mean value and standard deviation of the thrust and lateral force of the floating HAWTs and VAWTs. In the operation conditions LCs 1-8, notable differences among these floating wind turbines are found in the standard deviation of the thrust, as demonstrated in Figure 6a. The two-bladed floating VAWT gives significantly larger standard deviation in thrust than the others. Moreover, the standard deviation of the thrust of the three-bladed and four-bladed floating VAWTs are close to those of floating HAWTs, and they are all small compared to their mean values. It should also be noted that the floating VAWTs have large variations in the standard deviation of lateral forces, while the lateral forces of the floating HAWTs are close to zero, as shown in Figure 6b. In the parked condition LC 9, the blades of HAWTs were feathered and parallel to the wind direction, and this caused small thrust. The two-bladed VAWT was parked in a position that the blades are both parallel to the wind, which leads to very small thrust as well. Moreover, the drag forces acting on the tower for VAWTs are neglected, causing an almost zero thrust force. But for the three- and four-bladed VAWTs, the mean value of the thrust and lateral force are both very large.

For a floating wind turbine system that is subjected to the wind and wave loads, the platform motions and structural responses are of concern. Figure 7 demonstrates the mean values and standard deviations of pitch and yaw motions of the floating HAWTs and VAWTs. The mean pitch motions of floating HAWTs and VAWTs have similar trend as the mean thrust shown in Figure 6a. The considered floating VAWTs give a smaller pitch motion than the considered floating HAWTs in LCs 1-5. In LCs 6-8, though the thrust of floating VAWTs is larger, its torque arm of the pitch moment is smaller, leading to a more or less similar platform pitch motion as floating HAWTs. Moreover, the standard deviation of pitch motion of floating HAWTs is larger than those of floating VAWTs. The yaw motion, especially the mean yaw, presents prominent difference between the floating HAWTs and VAWTs. In operational condition, the

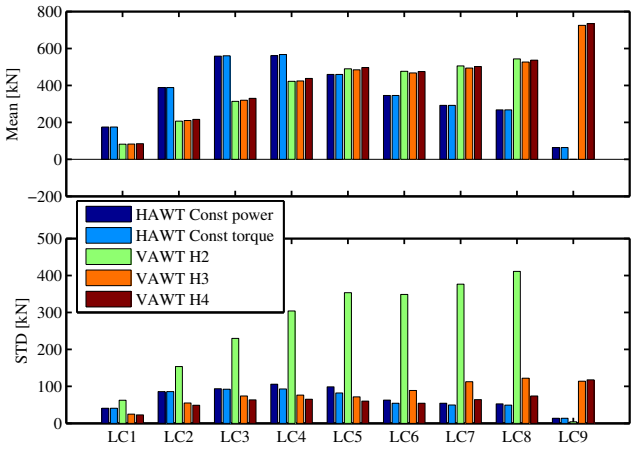

(a) Thrust

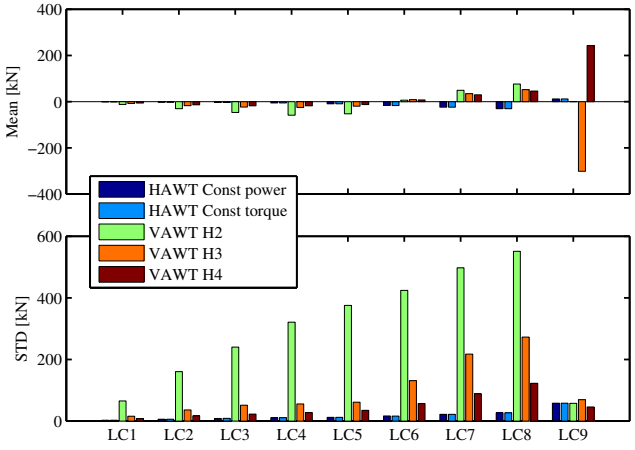

(b) Lateral force

Figure 6: The mean value and standard deviation of (a) thrust and (b) lateral force acting on the rotors for floating HAWT and VAWTs.

floating VAWTs have a considerable larger mean yaw than the floating HAWTs. This very large yaw motion is caused by the aerodynamic torque acting on the VAWTs, and has limited effect on the wind power capturing for the floating VAWTs. However, the standard deviations of the yaw motion between the floating VAWTs and HAWTs are fairly close compared to their mean value, as shown in Figure 7b. The floating VAWTs can give a smaller standard deviation

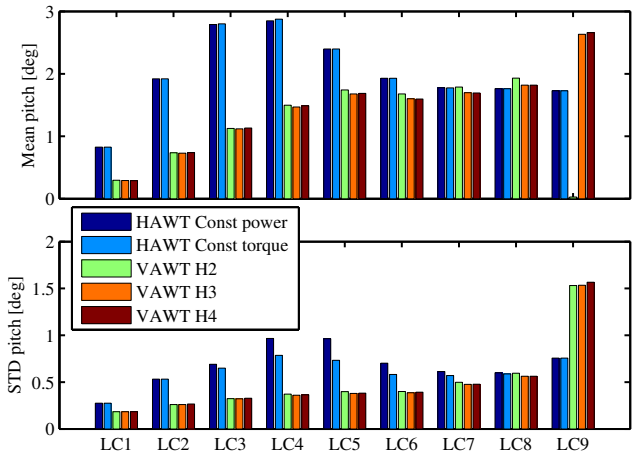

(a) Pitch

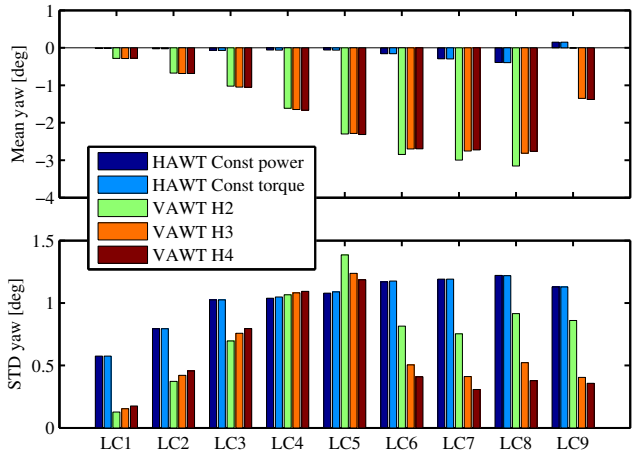

(b) Yaw

Figure 7: The mean value and standard deviation of (a) pitch and (b) yaw motions for floating HAWT and VAWTs.

in the yaw motion, especially in LCs 6-8. Regarding the parked condition LC 9, the two-bladed VAWT provides almost zero mean yaw motion, while the standard deviation of the yaw motion is quite large. The pitch and yaw motions for the three- and four-bladed VAWTs in the parked condition are very close.

The tower base bending moment is considered here as a representative structural response. The mean values and standard deviations of the tower base fore-

aft bending moment, M_{FA}, and side-side bending moment, M_{SS}, of the floating HAWTs and VAWTs are demonstrated in Figure 8. Regarding the mean value of M_{FA}, the floating HAWTs give a larger mean value in LCs 1-5, which are mainly due to two reasons: one is that they have larger thrust and longer torque arm, leading to a larger overturning moment; the other is that they have larger mean pitch motion, as shown in Figure 7a, making the mass of rotor contribute more to the fore-aft bending moment. The mean values of M_{SS} of both floating VAWTs and HAWTs are very small compared to the mean M_{FA}. In the parked condition, the two-bladed VAWT gives a tiny value of M_{FA} and M_{SS}, and the three- and four-bladed VAWTs provides much larger mean value of M_{FA} in the parked condition than in the operation condition, which implies that the extreme structural responses for the M_{FA} and M_{SS} are likely to occur in the extreme environmental condition.

The standard deviations of M_{FA} and M_{SS} of floating HAWTs differ very much with those of floating VAWTs, especially the floating VAWT with two blades, as illustrated in Figure 8. When the two-bladed VAWT rotates, the thrust varies from approximate zero to double of the mean value, causing significant variation in M_{FA} compared to the other wind turbines considered. The lateral force also varies periodically and significantly as the two-bladed VAWT rotates, resulting the considerable standard deviation of M_{SS}, as shown in Figure 8b. Furthermore, the standard deviations of M_{FA} of the three- and four-bladed floating VAWTs can be smaller than those of the floating HAWTs, while the standard deviation of M_{SS} of floating VAWTs are much larger than those of floating HAWTs.

The mooring line tension is also studied, as shown in Figure 9. The mooring line 2 that is parallel to the direction of wind and wave is considered here because it carries the largest tension among the three mooring lines. For the floating HAWTs, the mean values and standard deviations of the tension in mooring line 2 do not change too much at different LC. The floating VAWTs always have larger mean tension than the floating HAWTs. In the operation condition, the standard deviations of the tension are all small compared to their mean

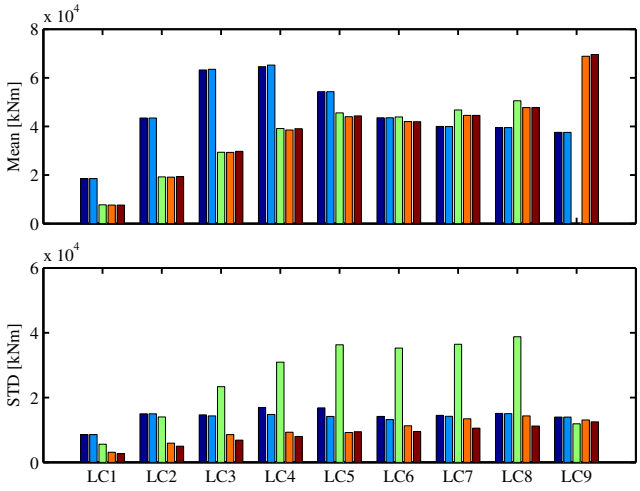

(a) Tower base fore-aft bending moment

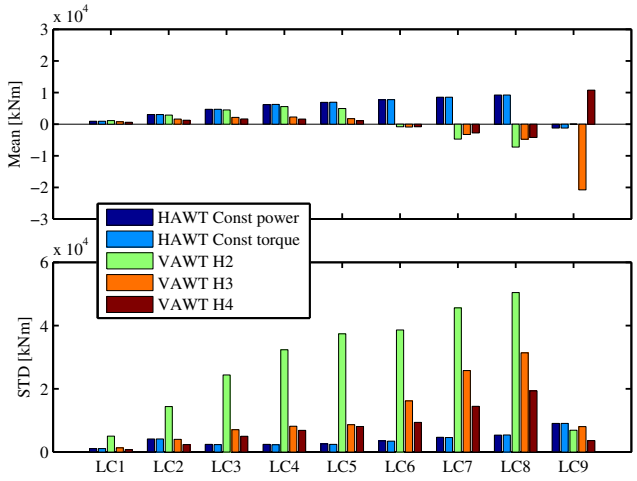

(b) Tower base side-side bending moment

Figure 8: The mean value and standard deviation of tower base (a) fore-aft bending moment and (b) side-side bending moment for floating HAWT and VAWTs.

values for all floating wind turbines. However, in the parked condition, the floating VAWTs, especially the three- and four-bladed VAWTs, have significant variations in the tension of mooring line 2.

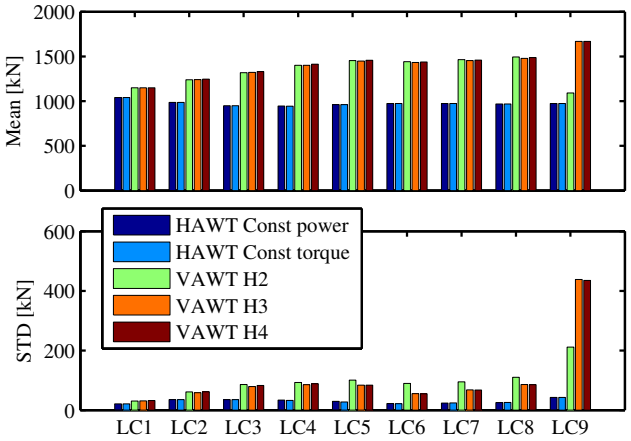

Figure 9: The mean value and standard deviation of the tension in mooring line 2 of the floating HAWTs and VAWTs.

5.3. Extreme structural responses of floating HAWTs and VAWTs

The extreme structural responses, such as the tower base bending moment and mooring line tension, of the floating HAWTs and VAWTs at each LC were studied in this section. The extreme value in a period of 1 h for each LC is predicted by applying the extrapolation of mean up-crossing rate method, as described in section 3.2.

To get a more straightforward comparison of the tower base bending moment between these floating HAWTs and VAWTs, the tower base bending moment, M, is simplified here using the instantaneous value as

$$M = \sqrt{(M_{FA}^2 + M_{SS}^2)} \tag{10}$$

An example time history of the tower base bending moment M of the three-bladed floating VAWT is presented in Figure 10. Figure 11 shows the example of extrapolation of up-crossing rate of the tower base bending moment for the floating HAWT and VAWT in LC4. As illustrated in Eq. 2, at a given period, different up-crossing rate level will give a different probability of exceedance. For a period of 1 h, the up-crossing rates of 10^{-4} and 10^{-5} give a probability of exceedance of approximately 30% and 3%, respectively. In this study, the max-

imum values presented are obtained using five 1 h realizations and extrapolated with an up-crossing rate of 10^{-4}.

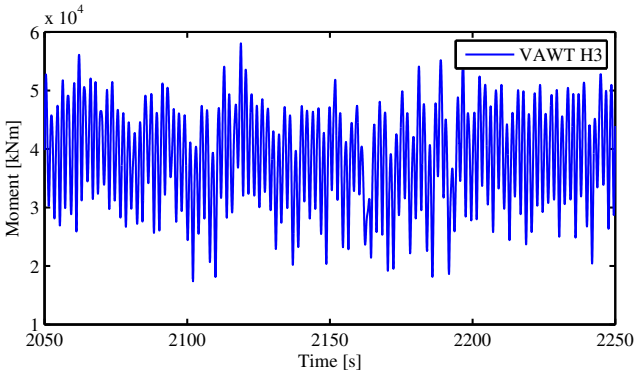

Figure 10: The time history of the tower base bending moment M for the three-bladed floating VAWT at LC4.

The maximum values of tower base bending moment of floating HAWTs and VAWTs are demonstrated in Figure 12. It can be observed that for the floating VAWTs, the two-bladed floating VAWT has extremely larger maximum value of tower base bending moment than the three- and four-bladed floating VAWTs in the operational condition. However, in the parked condition, the three- and four-bladed floating VAWTs have larger maximum values. This is because the two-bladed VAWT is parked at an azimuth angle that gives approximately zero thrust, while the three- and four-bladed VAWTs have relatively large thrust even though the azimuth angles that they parked give the smallest thrust, as presented in Figure 6a.

The potential LC that causes the largest tower base bending moment is different for these floating wind turbines. The two-bladed floating VAWT has the maximum at the LC with the cut-out wind speed; the floating HAWTs have the maximum at the LC with the rated wind speed; and the three- and four-bladed floating VAWTs have the maxim at the LC with extreme wind speed. Additionally, the maximum tower base bending moments of the three- and four-bladed floating VAWTs are very close to these of the floating HAWTs.

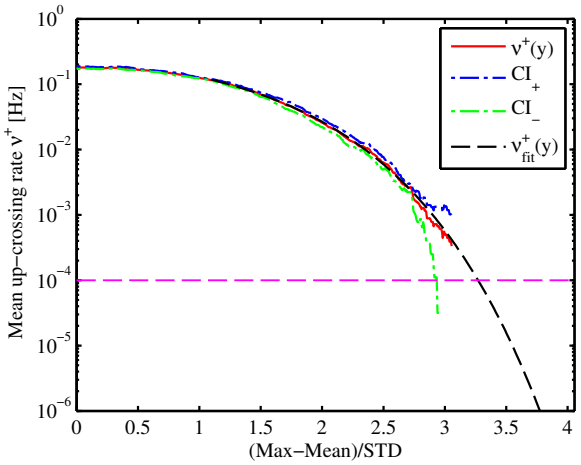

(a) Floating HAWT with constant torque in LC4

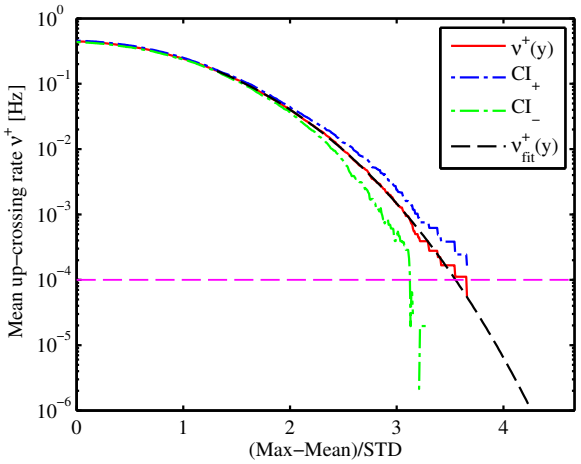

(b) Floating VAWT with three blades in LC4

Figure 11: Extrapolation of up-crossing rate of the tower base bending moment for (a) floating HAWT with constant torque in LC4 and (b) floating VAWT with three blades in LC4. Here $\nu^+(y)$ denotes the mean upcrossing rate computed by five realizations.

This implies that for the floating HAWTs and three- and four-bladed floating VAWTs considered, the floating VAWTs have comparable structural responses at the tower base as compared with floating HAWTs.

The maximum values of the tension in mooring line 2 for the floating HAWTs

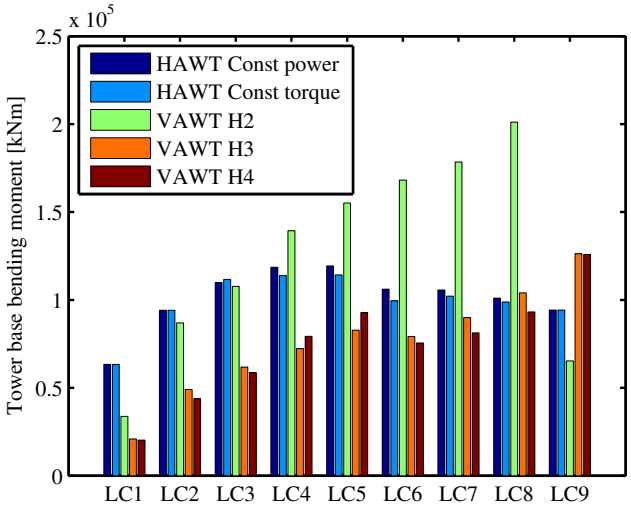

Figure 12: The maximum value of the tower base bending moment for the floating HAWTs and VAWTs.

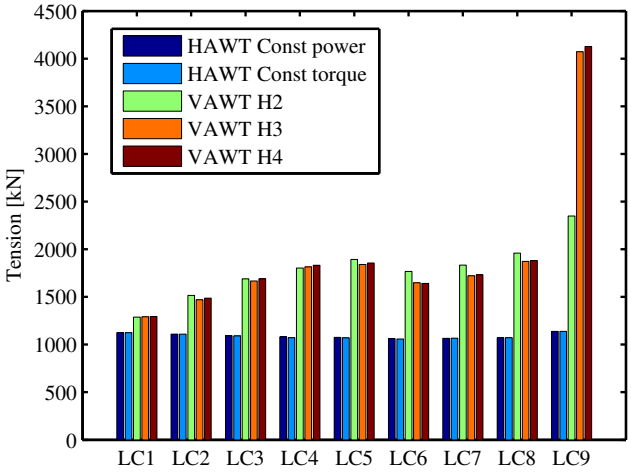

Figure 13: The maximum values of the tension in mooring line 2 for the floating HAWTs and VAWTs.

and VAWTs are presented in Figure 13. The floating VAWTs have larger maximum values in the tension than the floating HAWTs, especially in the parked condition. The maximum tension of the three- and four-bladed floating VAWTs is almost four times larger than those of the floating HAWTs, which means a

significant challenge for the design of mooring system.

5.4. Fatigue damage of floating HAWTs and VAWTs

Fatigue damage of floating HAWTs and VAWTs are represented by the DEFL described in section 3.3. Here both the 1Hz DEFL of the tower base fore-aft and side-side bending moments and tension in mooring lines are considered in the operational condition.

The 1Hz DEFLs of the tower base fore-aft bending moment, M_{FA}, and side-side bending moment, M_{SS}, of the floating HAWTs and VAWTs are demonstrated in Figure 14. Regarding the 1Hz DEFL of M_{FA} shown in Figure 14a, the two-bladed floating VAWT gives a considerably large value than other floating wind turbines, especially in LCs 3-8. Furthermore, the 1Hz DEFLs of M_{FA} of the three- and four-bladed floating VAWTs are even smaller than those of the floating HAWTs in LCs 1-4 with relatively low wind speeds and are comparable with those of the floating HAWTs in LCs 5-8. Since the long-term wind speeds commonly follow the Weibull distribution with the majority below 14 m/s [33], which corresponds to LC 5, the three- and four-bladed floating VAWTs have better fatigue damage performance at the tower base than the floating HAWTs in the fore-aft direction.

However, the fatigue damage of floating VAWTs in the lateral direction is much worse than that of floating HAWTs, as shown in Figure 14b. The 1Hz DEFL of M_{SS} of the two-bladed floating VAWT is several times larger than that of the floating HAWTs. For each LC in LCs 1-5, the 1Hz DEFL of M_{SS} of the three- and four-bladed floating VAWTs are very close to each other and are close to the corresponding 1Hz DEFL of M_{FA}. However, in LCs 6-8, the 1Hz DEFLs of M_{SS} of the three- and four-bladed floating VAWTs increases as wind speed increases, the 1Hz DEFL of M_{SS} of the three-bladed floating VAWT is observably larger than that of the four-bladed floating VAWT. Such increases are due to the effect of dynamic stall that the airfoil encounters. When the angle of attack is higher than a certain value, flow separation will occur on the airfoil and will affect lift and drag forces acting on the airfoil. In LCs 6-8

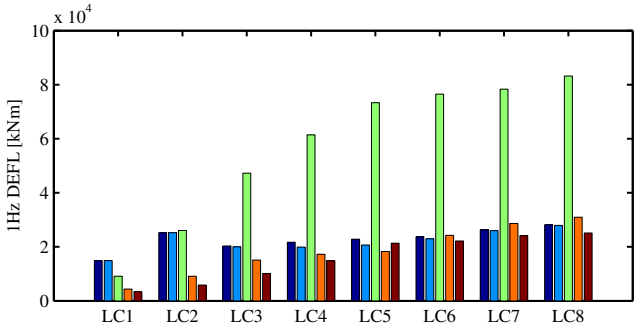

(a) 1Hz DEFL of tower base fore-aft bending moments

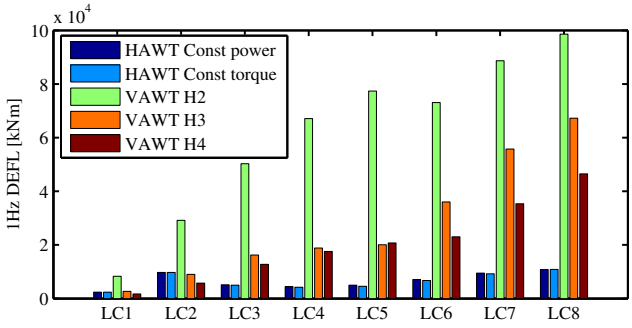

(b) 1Hz DEFL of tower base side-side bending moments

Figure 14: The 1Hz DEFL of tower base (a) fore-aft bending moment and (b) side-side bending moment for floating HAWT and VAWTs.

with high wind speed and low tip speed ratio, the angle of attack for each airfoil varies so significantly that such flow separation will happen at a large percentage during one rotation. Consequently, the resultant force resulting in the thrust and lateral force presents much larger fluctuation than LCs with high tip speed ratio. This will cause large 1Hz DEFL of M_{SS}, as those shown in Figure 14b.

As mentioned above, the long-term wind speeds are commonly below 14 m/s that corresponds to LC 5. As a result, the total fatigue damage at the tower base between the floating HAWTs and the three- and four-bladed floating VAWTs does not differ much.

The 1Hz DEFL of mooring line tensions of the floating HAWTs and VAWTs are also studied, as shown in Figure 15. The DEFLs in three mooring lines are

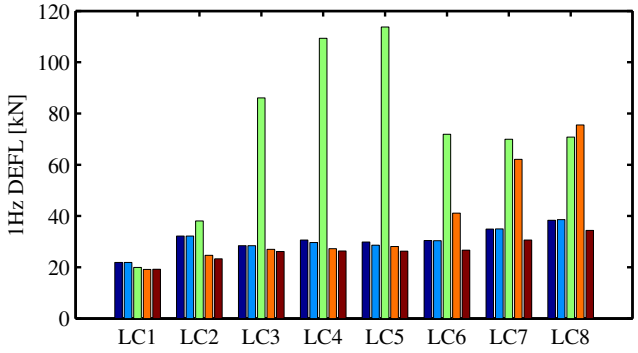

(a) 1Hz DEFL of tension in mooring line 1

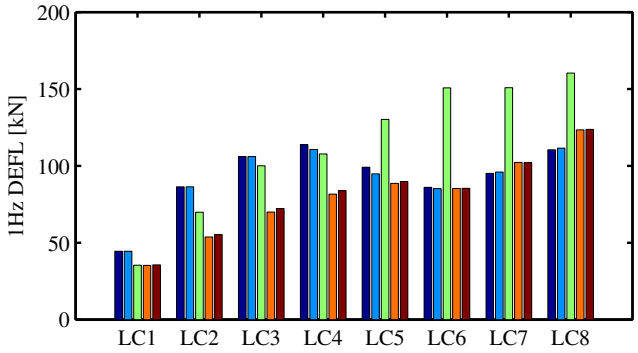

(b) 1Hz DEFL of tension in mooring line 2

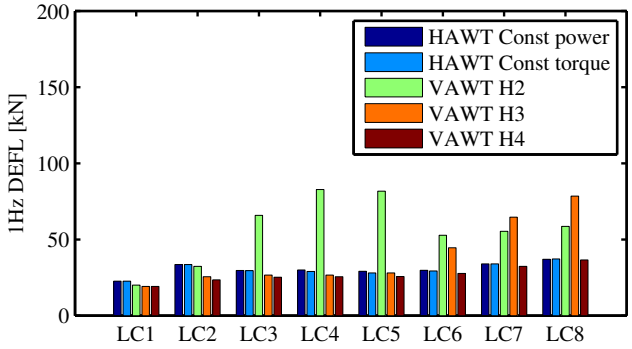

(c) 1Hz DEFL of tension in mooring line 3

Figure 15: The 1Hz DEFL of tension in mooring lines for floating HAWT and VAWTs for different load cases.

all considered. The mooring line 1 is in line with the wind and wave direction and carries the largest wind and wave loads. The mean value and standard deviation of tension in mooring line 1 are larger than those of mooring line 2 and 3. Also the 1 Hz DEFL in mooring line 1 is larger than that of mooring line 2 and 3 for the floating HAWTs and VAWTs. With respect to mooring line 1, the two-bladed floating VAWT give much larger 1Hz DEFL than the other floating wind turbines in LCs 5-8. In addition, the 1Hz DEFLs of tension in mooring line 1 of the three- and four-bladed floating VAWTs are smaller than those of floating HAWTs in LCs 1-4 and are close to them in LCs 5-8. Therefore, the fatigue damage of mooring line for the three- and four-bladed floating VAWTs are comparable with that of the floating HAWTs.

6. Conclusions

This study deals with the comparative study on the stochastic dynamic responses of floating horizontal axis wind turbines (HAWTs) and vertical axis wind turbines (VAWTs) with emphasis on the extreme structural responses and fatigue damages. The floating HAWTs with the NREL 5 MW three-bladed rotor, and the floating VAWTs with 5 MW straight-bladed H-rotors and with blade number ranging from two to four, both mounted on the OC4 semi-submersible platform, were considered. A series of time domain simulations in operational and parked conditions were carried out for the floating HAWTs and VAWTs using the fully coupled aero-hydro-servo-elastic codes SIMO-RIFLEX-AeroDyn and SIMO-RIFLEX-AC, respectively. The same turbulent wind and irregular wave conditions were applied. The stochastic dynamic responses, extreme structural responses and fatigue damages of the considered floating HAWTs and VAWTs were estimated and compared to reveal their merits and disadvantages.

The annual power production of the floating VAWTs is about 17.6% less than that of the floating HAWTs. The variations of the generator power production of floating VAWTs are comparable with that of floating HAWTs, except that the two-bladed floating VAWTs has a slightly larger variation in load cases (LCs)

with relatively high wind speed. In the operational condition, the standard deviations of the thrust of the three- and four-bladed floating VAWTs are close to those of floating HAWTs, and are much smaller than that of the two-bladed floating VAWT. Additionally, the mean values of tower base fore-aft bending moments of the three- and four-bladed floating VAWTs are smaller in LCs with low wind speeds and slightly larger in LCs with high wind speeds than that of floating HAWTs. And their standard deviations are slightly smaller than those of floating HAWTs. However, the standard deviations of tower base side-side bending moments of floating VAWTs are larger than that of floating HAWTs.

The maximum values of the tower base bending moment and mooring line tension are considered using the extrapolation of mean up-crossing rate method. The two-bladed floating VAWT has extremely large maximum value of tower base bending moment than the others. Moreover, the maximum tower base bending moments of the three- and four-bladed floating VAWTs are fairly close to that of the floating HAWTs, which implies that the considered floating VAWTs have comparable extreme structural responses at the tower base to the considered floating HAWTs. In addition, the maximum tensions in mooring line for the three- and four-bladed floating VAWTs are approximately four times as high as that of floating HAWTs, which means a big challenge for the design of mooring system.

The fatigue damage of tower base bending moment and mooring line tension are studied using the 1Hz damage equivalent fatigue loads (DEFLs). The two-bladed floating VAWT gives a considerably large value in the 1Hz DEFLs of both fore-aft and side-side bending moments than others. The 1Hz DEFLs of the tower base fore-aft bending moments of the three- and four-bladed floating VAWTs are smaller than those of the floating HAWTs in LCs with relatively low wind speeds and are comparable with those of the floating HAWTs in LCs with relatively high wind speeds. While the 1Hz DEFL of the tower base side-side bending moments of the three- and four-bladed floating VAWTs are slightly larger than that of floating HAWTs in LCs with relatively low wind speeds. However in general, the total fatigue damages at the tower base between the

floating HAWTs and the three- and four-bladed floating VAWTs are quite close. In addition, the fatigue damages of mooring line for the three- and four-bladed floating VAWTs are also comparable to that of the floating HAWTs.

It should be noted that the floating VAWTs used in this study are not optimal from an economical point of view, since the floating platform was initially designed to support the NREL 5MW wind turbine. However, they are still sufficient to demonstrate the inherent motion and structural response characteristics of floating VAWTs with different number of blades. As a whole, this study illustrates the dynamic response characteristics of four floating wind turbine concepts, highlights the merits and disadvantages of floating HAWTs and floating VAWTs, and can serve as a basis for their further development.

Acknowledgment

The authors would like to acknowledge the financial support from the EU FP7 project MARE WINT (project NO. 309395) and the Research Council of Norway through the Centre for Ships and Ocean Structures (CeSOS) and Centre for Autonomous Marine Operations and Systems (AMOS) at the Department of Marine Technology, Norwegian University of Science and Technology (NTNU), Trondheim, Norway.

References

[1] J. Paquette, M. Barone, Innovative offshore vertical-axis wind turbine rotor project, in: EWEA 2012 Annual Event, Copenhagen, Denmark, 2012.

[2] I. Paraschivoiu, Wind turbine design: with emphasis on Darrieus concept, Polytechnic International Press., Montreal, Canada., 2002.

[3] H. J. Sutherland, D. E. Berg, T. D. Ashwill, A retrospective of vawt technology, Tech. Report SAND2012-0304, Sandia National Laboratories, Albuquerque, New Mexico, USA (2012).

[4] Z. Cheng, Z. Gao, H. A. Madsen, T. Moan, Effect of the number of blades on the dynamics of floating straight-bladed vertical axis wind turbines, Renewable Energy 101 (2016) 1285–1298. doi:10.1016/j.renene.2016.09.074.

[5] Z. Cheng, K. Wang, Z. Gao, T. Moan, Dynamic response analysis of three floating wind turbine concepts with a two-bladed darrieus rotor, Journal of Ocean and Wind Energy 2 (2015) 213–222. doi:10.17736/jowe.2015.jcr33.

[6] Z. Cheng, Integrated dynamic analysis of floating vertical axis wind turbines, PhD thesis, Norwegian University of Science and Technology (2016).

[7] S. Eriksson, H. Bernhoff, M. Leijon, Evaluation of different turbine concepts for wind power, Renewable and Sustainable Energy Reviews 12 (5) (2008) 1419–1434. doi:10.1016/j.rser.2006.05.017.

[8] M. Borg, A. Shires, M. Collu, Offshore floating vertical axis wind turbines, dynamics modelling state of the art. part I : Aerodynamics, Renewable and Sustainable Energy Reviewsdoi:10.1016/j.rser.2014.07.096.

[9] M. Borg, M. Collu, A comparison between the dynamics of horizontal and vertical axis offshore floating wind turbines, Philosophical Transactions of the Royal Society of London A: Mathematical, Physical and Engineering Sciences 373 (2035) (2015) 20140076. doi:10.1098/rsta.2014.0076.

[10] K. Wang, C. Luan, T. Moan, M. O. L. Hansen, Comparative study of a FVAWT and a FHAWT with a semi-submersible floater, in: Proceedings of the 24th International Ocean and Polar Engineering Conference, Busan, South Korea, 2014.

[11] Z. Cheng, K. Wang, Z. Gao, T. Moan, Comparative study of spar type floating horizontal and vertical axis wind turbines subjected to constant winds, in: Proceedings of EWEA Offshore 2015, Copenhagen, Denmark, 2015.

[12] Z. Cheng, K. Wang, Z. Gao, T. Moan, A comparative study on dynamic responses of spar-type floating horizontal and vertical axis wind turbines, Wind Energydoi:10.1002/we.2007.

[13] U. S. Paulsen, M. Borg, H. A. Madsen, T. F. Pedersen, J. Hattel, E. Ritchie, C. S. Ferreira, H. Svendsen, P. A. Berthelsen, C. Smadja, Outcomes of the deepwind conceptual design, Energy Procedia 80 (2015) 329–341. doi:10.1016/j.egypro.2015.11.437.

[14] J. M. Jonkman, S. Butterfield, W. Musial, G. Scott, Definition of a 5-mw reference wind turbine for offshore system development, Tech. Rep. NREL/TP-500-38060, NREL, Golden, CO, USA (2009).

[15] A. Robertson, J. Jonkman, M. Masciola, H. Song, A. Goupee, A. Coulling, C. Luan, Definition of the semi-submersible floating system for phase II of OC4, Report (2012).

[16] H. Ormberg, E. E. Bachynski, Global analysis of floating wind turbines: Code development, model sensitivity and benchmark study, in: Proceedings of the 22th International Offshore and Polar Engineering Conference, Rhodes, Greece, 2012.

[17] Z. Cheng, H. A. Madsen, Z. Gao, T. Moan, A fully coupled method for numerical modeling and dynamic analysis of floating vertical axis wind turbines, Renewable Energy (2017) –doi:/10.1016/j.renene.2017.02.028.

[18] MARINTEK, Simo-theory manual version 4.0 (2012).

[19] MARINTEK, Riflex theory manual, version 4.0 (2012).

[20] P. J. Moriarty, A. C. Hansen, AeroDyn theory manual, NREL/TP-500-36881 (2005).

[21] H. Ormberg, E. Passano, N. Luxcey., Global analysis of a floating wind turbine using an aero-hydro-elastic model: Part 1 code development and

case study, in: Proceedings of the 30th International Conference on Ocean, Offshore and Arctic Engineering, 2011.

[22] H. A. Madsen, The Actuator Cylinder: A flow model for vertical axis wind turbines, Institute of Industrial Constructions and Energy Technology, Aalborg University Centre, 1982.

[23] Z. Cheng, H. A. Madsen, Z. Gao, T. Moan, Aerodynamic modeling of offshore vertical axis wind turbines using the actuator cylinder method, Energy Procedia 94 (2016) 531 – 543. doi:10.1016/j.egypro.2016.09.232.

[24] O. M. Faltinsen, Sea loads on ships and offshore structures, Cambridge University Press, Cambridge, UK, 1995.

[25] A. Naess, T. Moan, Stochastic dynamics of marine structures, Cambridge University Press, Cambridge, UK, 2012.

[26] W. Chai, A. Naess, B. J. Leira, Stochastic dynamic analysis and reliability of a vessel rolling in random beam seas, Journal of Ship Research 59 (2) (2015) 113–131.

[27] A. Naess, O. Gaidai, Monte carlo methods for estimating the extreme response of dynamical systems, Journal of Engineering Mechanics 134 (8) (2008) 628–636. doi:10.1061//ASCE/0733-9399/2008/134:8/628.

[28] A. Naess, O. Gaidai, P. S. Teigen, Extreme response prediction for nonlinear floating offshore structures by monte carlo simulation, Applied Ocean Research 29 (4) (2007) 221–230. doi:10.1016/j.apor.2007.12.001.

[29] W. Chai, A. Naess, B. J. Leira, G. Bulian, Efficient monte carlo simulation and grim effective wave model for predicting the extreme response of a vessel rolling in random head seas, Ocean Engineering 123 (2016) 191–203.

[30] G. Hayman, Mlife theory manual for version 1.00 (2012).

[31] B. J. Jonkman, Turbsim user's guide: Version 1.50. (2009).

[32] IEC, International standard 61400-3, wind turbines, part 3: Design requirements for offshore wind turbines (2009).

[33] K. Johannessen, T. S. Meling, S. Haver, Joint distribution for wind and waves in the northern north sea, International Journal of Offshore and Polar Engineering 12 (1).